FERMILAB-PUB-12-107-AD

DRAFT VERSION APRIL 18, 2012
Preprint typeset using LaTeX style emulateapj v. 2/16/10

COOLING AND HEATING FUNCTIONS OF PHOTOIONIZED GAS

NICKOLAY Y. GNEDIN[1,2,3] AND NICHOLAS HOLLON[2,3]

Draft version April 18, 2012

ABSTRACT

Cooling functions of cosmic gas are a crucial ingredient for any study of gas dynamics and thermodynamics in the interstellar and intergalactic medium. As such, they have been studied extensively in the past under the assumption of collisional ionization equilibrium. However, for a wide range of applications, the local radiation field introduces a non-negligible, often dominant, modification to the cooling and heating functions. In the most general case, these modifications cannot be described in simple terms, and would require a detailed calculation with a large set of chemical species using a radiative transfer code (the well-known code Cloudy, for example). We show, however, that for a sufficiently general variation in the spectral shape and intensity of the incident radiation field, the cooling and heating functions can be *approximated* as depending only on (1) the photo-dissociation rate of molecular hydrogen, (2) the hydrogen photo-ionization rate, and (3) the photo-ionization rate of O VIII; more complex and more accurate approximations also exist. Such dependence is easy to tabulate and implement in cosmological or galactic-scale simulations, thus economically accounting for an important but rarely-included factor in the evolution of cosmic gas. We also show a few examples where the radiation environment has a large effect, the most spectacular of which is a quasar that suppresses gas cooling in its host halo without any mechanical or non-radiative thermal feedback.

Subject headings: methods: numerical

1. INTRODUCTION

The ability of cosmic gas to radiate its internal energy (i.e. radiative cooling) and to absorb energy from the incident radiation field (radiative heating) is a primary distinction between the gas and dark matter; radiative heating and cooling processes are important in almost every study of gas dynamics or thermodynamics in the interstellar and intergalactic media. Because of this importance, cooling processes in the gas have been investigated in numerous prior studies, appear as central chapters in multiple textbooks, and are computed by several publicly available codes.

However, while the physics of radiative cooling and heating is well understood, the actual application of cooling and heating functions for studies of interstellar and intergalactic gas is surprisingly incomplete. The classic "standard cooling function" (e.g. Cox & Tucker 1969; Raymond et al. 1976; Shull & van Steenberg 1982; Gaetz & Salpeter 1983; Boehringer & Hensler 1989; Sutherland & Dopita 1993; Landi & Landini 1999; Benjamin et al. 2001; Santoro & Shull 2006; Gnat & Sternberg 2007; Smith et al. 2008) has indeed been computed and tabulated quite precisely. However, the "standard cooling function" is computed under the assumption of pure collisional ionization equilibrium (CIE), which is not always valid in the interstellar medium and is *never* valid in the intergalactic medium (c.f. Wiersma et al. 2009). In many astrophysical applications the incident radiation field introduces significant, often dominant, modifications to the "standard cooling function". On top of that, in some environments the assumption of the photoionization equilibrium may not be sufficiently accurate (Sutherland & Dopita 1993; Santoro & Shull 2006).

Such dependence can be illustrated by comparing the pure CIE cooling function with the cooling function in fully ionized gas, as shown in Figure 1 for both metal-free and solar-metallicity[4] gas. In the fully-ionized limit, where the only cooling process in bremsstrahlung, the cooling function over a wide range of temperatures differs from a pure CIE case by *more than two orders of magnitude*!

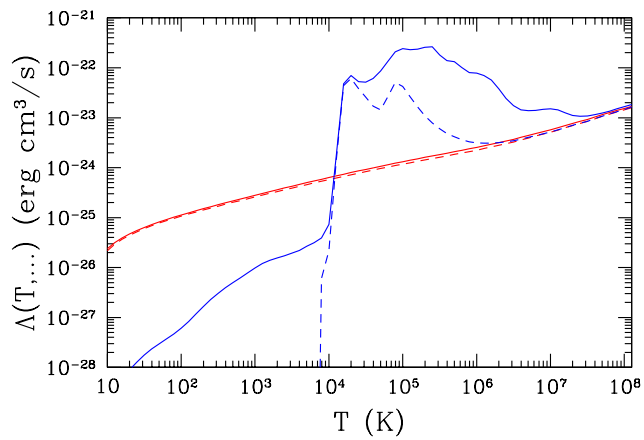

FIG. 1.— Example of the importance of the incident radiation field on the cooling functions: blue dashed and solid lines show the "standard cooling function" for the metal-free and solar-metallicity gas respectively. Corresponding red lines show the same cooling functions for the fully ionized gas.

Thus, the cooling function for photo-ionized gas depends not only on the gas temperature, number density, and metallicity, but also on the incident radiation field. There is, of course, nothing new in that statement. The crucial role of the radiation environment has always been understood by practitioners in the field. The challenge, however, is in economically accounting for this dependence in full 3D numerical simulations, where the cooling and heating functions are evaluated billions or even trillions of times during a single simulation.

[1] Particle Astrophysics Center, Fermi National Accelerator Laboratory, Batavia, IL 60510, USA; gnedin@fnal.gov

[2] Department of Astronomy & Astrophysics, The University of Chicago, Chicago, IL 60637 USA

[3] Kavli Institute for Cosmological Physics and Enrico Fermi Institute, The University of Chicago, Chicago, IL 60637 USA

[4] Throughout this paper, "solar metallicity" refers to the metallicity of the gas in the solar neighborhood, $Z \approx 0.02$, not the actual metallicity of the Sun.

Operated by Fermi Research Alliance, LLC under Contract No. De-AC02-07CH11359 with the United States Department of Energy.

If we allow for the worst case scenario – the radiation field J_ν is allowed to vary arbitrarily – we can introduce sharp edges and features in the radiation spectrum that are specially designed to ionize particular levels of particular elements. This allows the cooling function to be "sculpted" in an essentially arbitrary way.

One possible way to account for the effect of the incident radiation field is to fix the radiation spectrum and amplitude. For example, in studies of intergalactic medium it is often (but not always) sufficient to account for the cosmic background radiation. Since the cosmic background radiation evolves with redshift, the cooling and heating functions become redshift-dependent, but such 1-dimensional dependence is easy to pre-compute and tabulate for use in simulations (Benson et al. 2002; Kravtsov 2003; Wiersma et al. 2009; Vasiliev 2011). Unfortunately, these cooling and heating rates are then often used for modeling gas dynamics in galactic halos or even ISM – environments where the cosmic background radiation is a sub-dominant component of the incident radiation field.

Therefore, it is desirable to find a way to account for a general shape of the incident radiation field without the need to recompute the cooling and heating functions every time they are needed. In this paper, we show that it is possible to come up with an approximate solution for this problem using a sufficiently general model for the radiation field spectrum.

2. APPROXIMATING THE COOLING AND HEATING FUNCTIONS

The radiative term in the internal energy equation - the rate of change of the gas internal energy due to radiative gains and losses - can be represented as

$$\left.\frac{dU}{dt}\right|_{\rm rad} = n_b^2\left[\Gamma(T,...)-\Lambda(T,...)\right], \qquad (1)$$

where U is the gas thermal energy and $n_b = n_{\rm H}+4n_{\rm He}+..$ is the total baryon number density. We explicitly factored out n_b^2 in both the cooling (Λ) and the heating (Γ) functions so that these are density-independent in the CIE limit.

In the most general case the cooling and heating functions depends on an extremely large set of arguments: gas temperatute T, baryon number density n_b (in addition to n_b^2 depedence explicitly accounted for in Equation (1)), the fractional abundance X_{ij} for the species i (inclouding atomic and ionic species, various molecules, and cosmic dust) at level j, the distribution of the column density for the species i at level j at different velocity values with respect to the systemic velocity $dN_{ij}(v)/dv$, the specific intensity of the radiation field as a function of frequency J_ν, and the heating rate by cosmic rays $\zeta_{\rm CR}$,

$$\mathcal{F}(T,...) = \mathcal{F}(T,n_b,X_{ij},\frac{dN_{ij}(v)}{dv},J_\nu,\zeta_{\rm CR}), \qquad (2)$$

where hereafter $\mathcal{F}$ denotes either Γ or Λ,

$$\mathcal{F}(...) \equiv \left[\begin{array}{l}\Gamma(...)\\ \Lambda(...)\end{array}\right. .$$

Obviously, such a complex dependence cannot be described in simple terms, and would require a detailed calculation with a large set of chemical species using a radiative transfer code - for example, the well-known code Cloudy (Ferland et al. 1998). That would make it impractical as a method for computing the cooling and heating function in realistic three-dimensional numerical simulations.

We, therefore, adopt several major simplifications. First, we restrict our focus to a purely optically thin case (all $N_{ij}=0$). That immediately implies that we have to explicitly exclude cooling and heating due to molecules and dust - these processes crucially depend on radiative transfer and computing them in the optically thin case does not make much physical sense (molecular clouds are shielded). We also exclude cosmic rays, since cosmic ray heating is mostly important in molecular gas, which we exclude anyway.

With these restrictions, Equation (2) becomes

$$\mathcal{F}(T,...) = \mathcal{F}(T,n_b,X_{ij},J_\nu).$$

Even that is way too complex, as the cooling and heating functions depend on hudreds of individual level populations for atomic and ionized species.

At low enough densities and faint enough incident radiation fields, most of reactions that result in cooling and heating in gas are interactions of an atom/ion with either a photon or an electron. Hence, in this limit cooling and heating functions (Eq. 1) can be substantially simplified:

$$\mathcal{F}(T,n_b,Z,J_\nu) \approx \left.\mathcal{F}(T,Z,\frac{J_\nu}{n_b})\right|_{n_b,J_\nu\to 0},$$

For example, this is case for the "standard cooling function", which is density independent in our convention of Equation (1).

Unfortunately, this approximation is only valid for impractically low values of the radiation field; it is invalid, for example, in typical ISM conditions in the Milky Way. Not only do various 3-body processes become important at high densities, but a realistic radiation environment will cause some of the excited states of various atoms and ions to become populated. Collisional de-excitation of excited levels breaks the density-independence of the cooling and heating functions.

Of course, when some of the radiation emitted by the gas is trapped, radiative transfer effects become important, and cooling and heating functions become dependent not only on the gas density, but also on the overall spatial distribution of the emitting gas. In other words, the whole concept of cooling and heating functions becomes invalid.

We enforce this by restricting Cloudy calculations to a single zone and setting the zone size to a vanishingly small value. The collisional de-excitation and 3-body reactions still induce an explicit density dependence in the cooling and heating functions, but this dependence is not strong (linear at most) if we parameterize the functions as

$$\mathcal{F}(T,n_b,Z,J_\nu) = \mathcal{F}(T,Z,\frac{J_\nu}{n_b},n_b). \qquad (3)$$

3. MODELING THE INCIDENT RADIATION FIELD

As we mentioned above, it is not possible to account parametrically for an arbitrary radiation field spectrum. However, in a vast majority of astrophysical application the incident radiation field is dominated by radiation from stars, AGN or a combination thereof. Thus, we model the incident radiation field as

$$J_\nu = J_0 e^{-\tau_\nu}\left[\frac{1}{1+f_Q}s_\nu + \frac{f_Q}{1+f_Q}x^{-\alpha}\right], \qquad (4)$$

where x is the photon energy in Rydbergs ($x \equiv h\nu/(1\,{\rm Ry})$), and s_ν is a fit to the stellar spectrum from Starburst99 (Lei-

therer et al. 1999),

$$s_\nu = \frac{1}{5.5}\begin{cases} 5.5, & x<1 \\ x^{-1.8}, & 1<x<2.5 \\ 0.4x^{-1.8}, & 2.5<x<4 \\ 2\times10^{-3}x^3/\left(\exp(x/1.4)-1\right), & 4<x \end{cases}$$

(this fit is shown in Fig. 4 of Ricotti et al. (2002)). Equation (4) also includes the possibility that the incident radiation field is attenuated by gas with the opacity

$$\tau_\nu = \frac{\tau_0}{\sigma_{\rm HI,0}}\left[0.76\sigma_{\rm HI}(\nu)+0.06\sigma_{\rm HeI}(\nu)\right],$$

where $\sigma_j(\nu)$ and $\sigma_{j,0}$ are photoionization cross-sections and their values at respective ionization thresholds for $j = $ H I and He I, and τ_0 is a parameter.

Overall, the radiation field model from Equation (4) contains 4 parameters: the amplitude J_0, the AGN-like power-law contribution slope α and amplitude f_Q, and the shielding optical depth τ_0. The last 3 parameters are dimensionless; we choose to measure J_0 in units of the typical radiation field in the Milky Way galaxy, $J_{\rm MW} = 10^6$ photons cm^{-2} s^{-1} ster^{-1} eV^{-1} (Draine 1978; Mathis et al. 1983).

For each set of parameters, we use the widely known photoionization code Cloudy (Ferland et al. 1998) to compute the cooling and heating function for a range of gas temperatures at fixed gas density and metallicity. Examples of such computations are shown in Figure 2. For all 3 cases the radiation field is the same at 1 Ry, but differs in spectral shape at other frequencies (a stellar spectrum, a power-law spectrum, and a power-law spectrum shielded by a $\tau_0 = 100$ cloud).

In order to extensively explore the cooling and heating functions for our radiation field model, we sampled the full parameter space (metallicity, density, and the radiation field) on the following grid of values:

$$\begin{aligned} Z/Z_\odot &= 0, 0.1, 0.3, 1, 3 \\ \lg(n_b/\,{\rm cm}^{-3}) &= -6, -5, ..., 6 \\ \lg(J_0\,{\rm cm}^{-3}/n_b/J_{\rm MW}) &= -3, -2.5, -2, ..., 7 \\ \alpha &= 1, 1.5, 2, 2.5, 3 \\ \lg(f_q) &= -3, -2.5, -2, ..., 1 \\ \lg(\tau_0) &= -1, -0.5, 0, ..., 3 \end{aligned} \tag{5}$$

This parameter range is wide enough to include both extremes shown in Fig. 1: the case where the radiation field is completely negligible and the case where the gas is fully photoionized.

For each of the $5\times13\times21\times5\times9\times9 \approx 550{,}000$ sets of parameters from this grid, we run Cloudy to compute the cooling and heating functions for 81 values of the temperature between 10 K and 10^9 K in steps of 0.1 dex (almost 45 million Cloudy runs altogether). Using this large database, we now consider the various dependencies of the cooling and heating functions one by one.

3.1. *Metallicity Dependence*

In a further simplification, we expand both cooling and heating functions into Taylor series in metallicity up to the quadratic term,

$$\mathcal{F} \approx \mathcal{F}_0 + \frac{Z}{Z_\odot}\mathcal{F}_1 + \left(\frac{Z}{Z_\odot}\right)^2\mathcal{F}_2, \tag{6}$$

where all functions Γ_i and Λ_i depend only on T, J_ν/n_b, and n_b.

We achieve this decomposition in practice by fitting a second degree polynomial to the five Z values that we sample in Table (5). This, and all of our subsequent approximations, we extensively test below in §4. Here we note simply that the error introduced by dropping cubic and higher power terms is by far the smallest of the errors introduced by our approximations – in the rms sense, the second order expansion of the Taylor series is accurate to better than 3% – as long as we restrict Z to less than 3 solar metallicities. The quadratic approximation rapidly loses accuracy as the metallicity increases. At metallicities above $5Z_\odot$, approximation (6) even results in negative cooling functions in a few instances.

Six functions Γ_i and Λ_i ($i = 0, 1, 2$) can be used directly, but since cooling and heating functions are not necessarily monotonic functions of Z, some of $\mathcal{F}_1$ and $\mathcal{F}_2$ (again, $\mathcal{F}$ stands for either Γ or Λ) can be negative. Since interpolation in log-log space is usually more accurate than direct interpolation, positive functions are much more suitable for tabulation and interpolation. Hence, we replace 6 functions $\mathcal{F}_i$ with 6 new functions $\tilde{\mathcal{F}}_i$ as

$$\begin{aligned} \tilde{\mathcal{F}}_0 &= \mathcal{F}_0, \\ \tilde{\mathcal{F}}_1 &= \mathcal{F}_0 + \mathcal{F}_1 + \mathcal{F}_2, \\ \tilde{\mathcal{F}}_2 &= \mathcal{F}_0 + 2\mathcal{F}_1 + 4\mathcal{F}_2, \end{aligned}$$

where symbol $\tilde{\mathcal{F}}$ also means either the cooling or the heating function. Functions $\tilde{\mathcal{F}}_i$ are none other than the cooling and heating functions at $Z = i\times Z_\odot$ and hence are always positive. The transformation between $\mathcal{F}_i$ and $\tilde{\mathcal{F}}_i$ is linear and can be trivially inverted.

In the following, we always operate on functions $\tilde{\mathcal{F}}_i$ and convert them back to $\mathcal{F}_i$ (i.e. Γ_i and Λ_i) as the very last step.

3.2. *Radiation Field Dependence*

So far we still have not resolved the main challenge – the fact that the 6 functions $\tilde{\mathcal{F}}_i$ that we need to describe depend on the whole incident radiation field J_ν,

$$\tilde{\mathcal{F}}_i = \tilde{\mathcal{F}}_i(T, \frac{J_\nu}{n_b}, n_b).$$

The primary contribution of this paper is that we further approximate this dependence by replacing the full radiation field with a finite set of photoionization rates.

Specifically, let us define a normalized rate Q_j as

$$Q_j \equiv \frac{P_j}{n_b},$$

where P_j is a photoionization rate for some atom or ion. We now seek an approximation of the form

$$\tilde{\mathcal{F}}_i(T, \frac{J_\nu}{n_b}, n_b) \approx \tilde{\mathcal{F}}_i(T, Q_j, n_b) \tag{7}$$

for $i = 0, 1, 2$ and some set of Q_j.

It makes sense that the rates we choose to represent the radiation field should sample the wide range of frequencies. For example, since C II is an important coolant in the low-temperature regime, one of the rates should sample the radiation field below the hydrogen ionization threshold. We choose the photo-dissociation rate of molecular hydrogen in the Lyman-Werner band as such a rate, simply because that

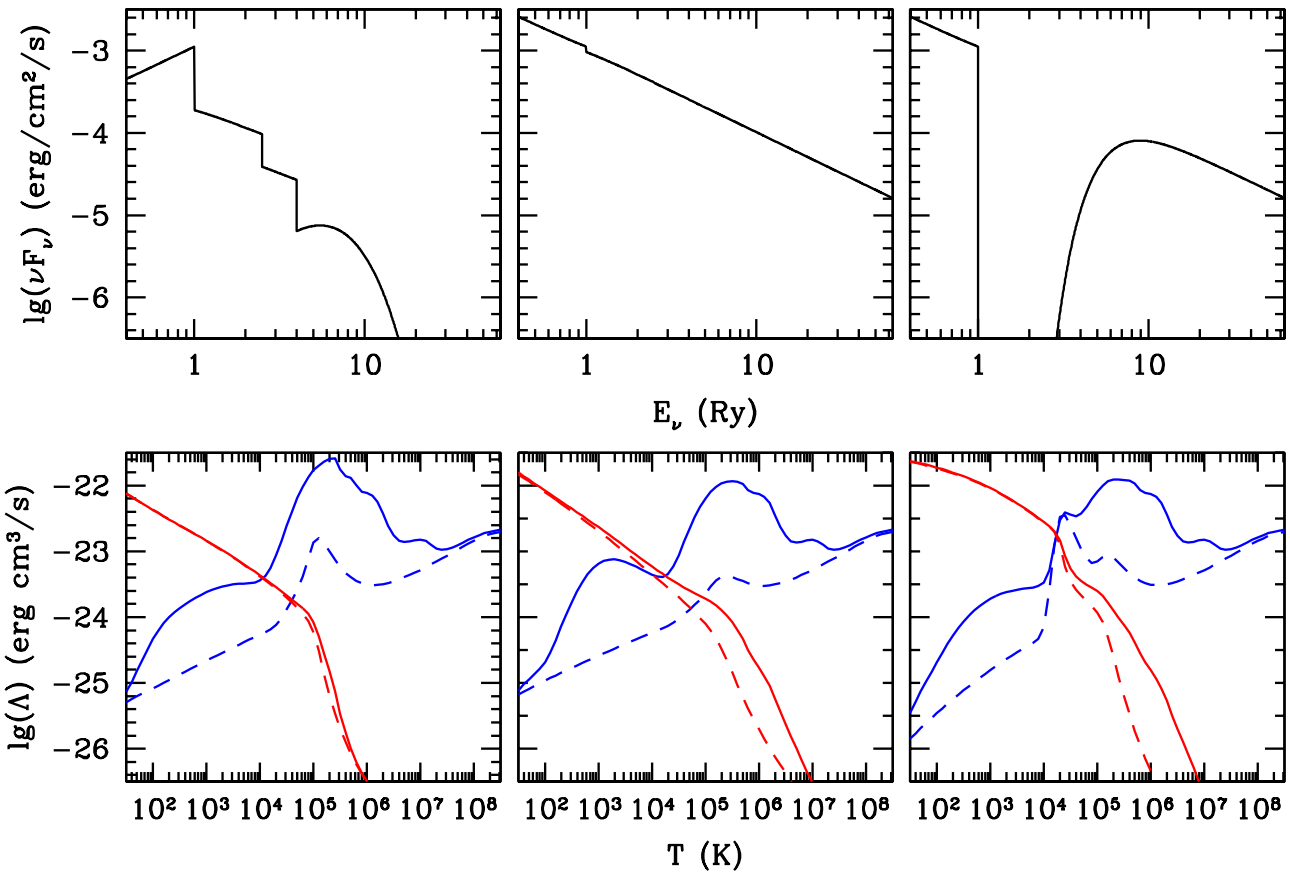

FIG. 2.— Incident radiation fields (top panels) and gas cooling (blue lines) and heating (red lines) functions (bottom panels) for three different radiation field models: $[J_0, \alpha, f_Q, \tau_0] = [100J_{\rm MW}, 3, 10^{-3}, 0.1]$ (left), $[100J_{\rm MW}, 2, 10, 0.1]$ (middle), and $[100J_{\rm MW}, 2, 10, 100]$ (right), all for $n_{\rm H} = 1\,{\rm cm}^{-3}$. As in Fig. 1, solid and dashed lines are for $Z = 0$ and $Z = Z_\odot$ respectively. It is clear that the cooling and heating functions are strongly dependent on the incident radiation field.

rate is also useful for several other processes that can be modeled in the numerical code (for example, the destruction of molecular hydrogen). It also makes sense to use the hydrogen ionization rate since hydrogen is an important coolant at $T \gtrsim 10{,}000$ K for all but the highest radiation fields. Finally, one of the selected rates should be sensitive to high energy photons.

We present two specific choices for Q_j in §3.4.

3.3. *Density Dependence*

Finally, we need to address the remaining density dependence in Equation (7). The trick of using Q_j makes this dependence relatively weak, although highly non-trivial. We adopt two strategies to deal with it. The first one is the simplest possible approach – we tabulate $\tilde{\mathcal{F}}_i$ at the 13 density values we tested in Table (5) and linearly interpolate in log-log space. The guaranteed positiveness of $\tilde{\mathcal{F}}_i$ becomes crucial when working in logarithmic space.

In the second approach we fit the density dependence of $\tilde{\mathcal{F}}_i$ with the following fitting formula:

$$\tilde{\mathcal{F}}_i(T, Q_j, n_b) \approx \frac{a^2 + abn_b^{\beta} + b^2 n_b^{2\beta}}{1 + cn_b^{\gamma} + c^2 n_b^{2\gamma}} + dn_b, \qquad (8)$$

where all fitting parameters $(a, b, c, d, \beta, \gamma)$ depend on i, T, and all Q_j. The last term with non-negative d describes the 3-body reactions (hence an extra n_b power on top of the two already factored out in Equation 1), while the first term describes the effect of collisional de-excitation. Its particular functional form is not motivated by any physical considerations, but we find empirically that it works well. In addition, this functional form guarantees that all $\tilde{\mathcal{F}}_i$ remain positive for any vale of n_b, even outside of our tested range.

Using the "density-interpolated" approach uses more memory (13 density values) but is faster; the "density-fitted" approach of Equation (8) is more economical (just 6 fit parameters) but requires evaluating the complex formula for every function evaluation and hence is several times slower. As we show below in §4, they are essentially identical in their numerical precision. Thus, the two approaches offer an optimization choice between speed and memory in a numerical implementation.

3.4. *Notes on the Specific Implementations*

In this paper we consider two primary implementations. In the first implementation we take three values $Q_{\rm LW}$, $Q_{\rm H\,I}$, and $Q_{\rm O\,VIII}$, combine them into 3 parameters

$$\begin{aligned} r_1 &= Q_{\rm LW}, \\ r_2 &= Q_{\rm H\,I}/Q_{\rm LW}, \\ r_3 &= Q_{\rm O\,VIII}/Q_{\rm LW}, \end{aligned} \qquad (9)$$

and call this implementation the "LHO table". In this implementation the particular choice of the third rate is not very important; any hydrogenic sequence rate for elements from oxygen to aluminum (F IX, Ne X, ..., Al XIII) gives an almost equivalent approximation.

In the second, "LHOSI table" approximation, we use 5 separate rates combined into 4 parameters:

$$\begin{aligned} r_1 &= Q_{\rm LW}, \\ r_2 &= Q_{\rm H\,I}/Q_{\rm LW}, \\ r_3 &= Q_{\rm O\,VIII}/Q_{\rm LW}, \\ r_4 &= Q^{0.1}_{\rm S\,XVI} Q^{0.9}_{\rm Fe\,XXVI}/Q_{\rm O\,VIII}. \end{aligned} \tag{10}$$

This approximation is expected to be more accurate that the 3-rate LHO one, but it is more complex. We have manually explored a substantial set of possible choices for Q_j, but have not conducted a fully exhaustive search, as it would require complex automation of the search process.

We implement each of the two approximations (7) by constructing a grid of parameter values and computing the average cooling and heating functions for all incident radiation fields that give the same set of parameter values r_j.

For the LHO table, we use a logarithmically-spaced table for $-12.5 \le \lg(r_1) \le -3$, $-6.5 \le \lg(r_2) \le 0$, and $-9.5 \le \lg(r_3) \le -3.5$ with the logarithmic step of 0.5 dex. We found that using a finer step in the table does not lead to any increase of accuracy. Such a table for a single value of the gas density includes $20 \times 14 \times 13 = 3640$ entries. A full table that uses 13 density values for the "density-interpolated" implementation takes 88 MB of memory. A slower, "density-fitted" implementation takes only 40 MB of memory.

Our implementation of the LHOSI table uses the same spacing and parameter ranges for r_1, r_2, and r_3 (which are the same as in the LHO table); for the last parameter it adopts a range of $-3.5 \le \lg(r_4) \le -2$. The resulting table contains $20 \times 14 \times 13 \times 4 = 14{,}560$ entries. A full table that uses 13 density values for the "density-interpolated" implementation takes 350 MB of memory. A slower, "density-fitted" implementation takes about 160 MB of memory.

4. TESTING THE COMPLETE APPROXIMATION

Since we use our sample of Cloudy runs to create the actual tables with the cooling and heating functions, we need a different data set to test the accuracy of our approximations. For this purpose we select 100,000 points from within our parameter space (5), sampling uniformly on a logarithmic scale (for the metallicity, we randomly choose a value between -3 and 0.5 in $\lg(Z)$). For each test point, we run Cloudy for our 81 values of the temperature to compute cooling and heating functions. This "testing" data set is completely independent of the data set used to create the tables.

We show in Figure 3 the error distribution for two implementations (LHO and LHOSI) described above. Two features of Fig. 3 are important to note. First, the median errors for both cooling and heating functions are modest, less than 10%. This is very good news indeed, as it shows that the whole diversity of cooling and heating functions can be parametrized economically, albeit approximately. Second, unfortunately, is that the error distribution is not Gaussian, but rather exhibits a long tail toward large, or "catastrophic", errors. For example, in 1% of all cases that we tested, the errors in the LHO approximation reach a factor of 2. The LHOSI approximation is better, but still exhibits catastrophic errors.

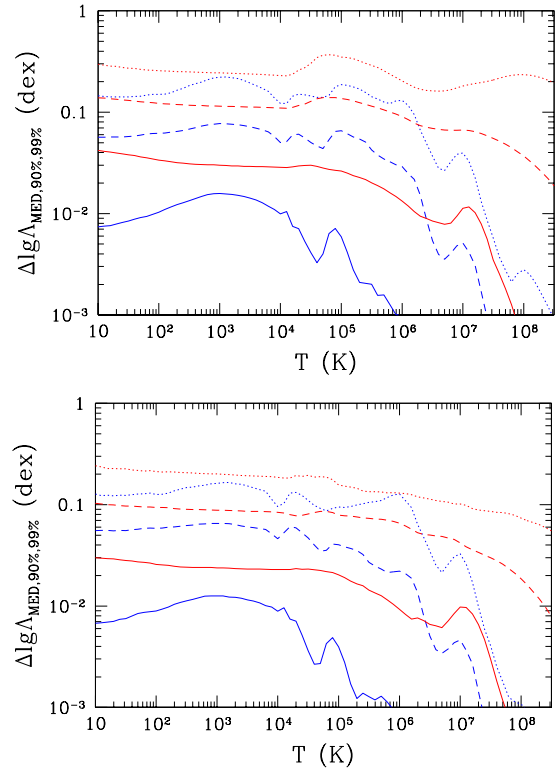

FIG. 3.— Error in approximating the cooling (blue lines) and heating (red lines) functions with several photoionization rates. Solid lines trace the median error (50% of cases have the error below the solid line), dashed lines trace the 90% error, and dotted line trace the 99% error (only 1% of all cases have an error above the dotted line). The top panel shows the LHO table and the bottom shows the LHOSI table. The existence of "catastrophic" errors (a small number of cases with large errors) is apparent from this figure.

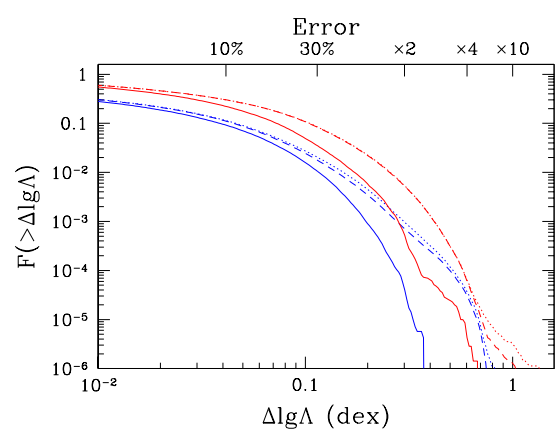

FIG. 4.— Cumulative error distributions for all values of gas temperatures for the heating (red lines) and cooling (blue lines) functions for 3 approximations: density-fitted LHO (dotted lines), density-interpolated LHO (dashed lines), and density-interpolated LHOSI (solid lines).

In both cases, the lines for the "density-interpolated" and "density-fitted" variants of both tables are virtually indistinguishable from each other because the errors are completely dominated by the inaccuracy of our main ansatz (7). This is also illustrated in Figure 4, where we show the cumulative error distribution for all temperature values for the density-interpolated LHOSI table and both the density-interpolated and density-fitted variants of the LHO table. For one case in a million, the LHO table reaches an error factor of 10. For the

LHOSI table that error is a factor of 4 for the heating function and only a factor of 2 for the cooling function.

Of course, the specific shape of the distributions shown in Fig. 4 is only applicable to our adopted uniform sampling. For a specific numerical simulation, the probability of errors of a particular magnitude will depend on the simulation details and cannot be predicted a priori.

5. CONCLUSIONS

Our main result is that one can *approximately* represent the most general cooling and heating functions for gas in ionization equilibrium as

$$\{\Gamma,\Lambda\}(T,n_b,Z,J_\nu) \approx \sum_{i=0}^{2}\left(\frac{Z}{Z_\odot}\right)^i \{\Gamma,\Lambda\}_i(T,r_j,n_b) \quad (11)$$

with $r_1 = P_{\rm LW}/n_b$, $r_2 = P_{\rm HI}/P_{\rm LW}$, and $r_3 = P_{\rm O\,VIII}/P_{\rm LW}$ (the LHO approximation), or more accurately with the more complex LHOSI approximation (10). These approximations are rather accurate on average, but suffer from "catastrophic" errors – in 10^{-6} of all cases the approximate cooling or heating function may deviate from the exact calculation by up to a factor of 4 for the LHOSI approximation and a factor of 10 for the LHO approximation. Thus, these approximations are not suitable for all applications.

Equation (11) does capture the qualitative dependence of the cooling and heating functions on the incident radiation field. To illustrate this, we show in the appendix three examples where the cooling and heating functions are significantly modified by the incident radiation field. The last example – the quasar irradiating its own galactic halo (§A.3) – not only shows an alteration to the cooling/heating functions, but actually presents a novel feedback mechanism: the central black hole suppresses the gas accretion from the halo without any additional mechanical or thermal feedback.

We are grateful to Andrey Kravtsov for enlightening discussions and constructive criticism. This work was supported in part by the DOE at Fermilab, by the NSF grant AST-0908063, and by the NASA grant NNX-09AJ54G. The calculations used in this work have been performed on the Joint Fermilab - KICP Supercomputing Cluster, supported by grants from Fermilab, Kavli Institute for Cosmological Physics, and the University of Chicago. We acknowledge the use of code Cloudy (Ferland et al. 1998) as the primary research tool of this study. This work made extensive use of the NASA Astrophysics Data System and `arXiv.org` preprint server.

APPENDIX

SOME EXAMPLES OF COOLING AND HEATING FUNCTIONS IN ISM AND IGM

In this section we present a few examples where the incident radiation field significantly affects the cooling and heating rates in the gas. These examples are *not* real physical models, but are simple demonstrations that the dependence that we explore in this paper actually matters.

The examples presented here are not exhaustive, of course; one can imagine many other similar situations. Their purpose is to illustrate the numerous possible feedback effects in interstellar and intergalactic environments that arise when we take into account the effects gas metallicity and incident radiation field on the cooling and heating rates. These effects can be studied, even if only semi-quantitatively, with the approximations presented in this paper.

Galactic Halo Near a Quasar

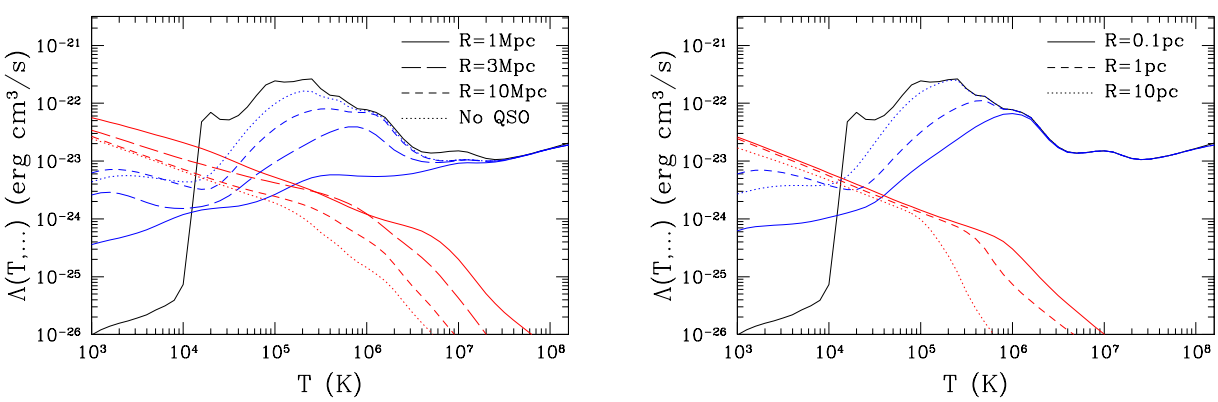

FIG. 5.— *Left*: Cooling (blue lines) and heating (red lines) functions for a $Z = Z_\odot$, $n_b = 340 \times \bar{n}_b$ galactic halo at the specified distances from a quasar with an ionizing luminosity $10^{13} L_\odot$. The black solid line shows the pure CIE "standard cooling function". *Right*: Cooling (blue lines) and heating (red lines) functions for a $Z = Z_\odot$, $n_b = 1\,{\rm cm}^{-3}$ HII region around an O star. The black solid line shows the pure CIE "standard cooling function".

In the left panel of Figure 5 we show cooling and heating functions for a typical galactic halo at $z = 0$ ($n_b = 340 \times \bar{n}_b = 8.5 \times 10^{-5}\,{\rm cm}^{-3}$) surrounding a bright quasar with an ionizing luminosity of $10^{13} L_\odot$ (roughly corresponding to a $10^9 M_\odot$ black hole). We assume solar metallicity, a quasar spectrum of $J_\nu \propto \nu^{-2}$, and the Haardt & Madau (2001) background.

Some interesting consequences may arise from the radiation-field-dependence of the cooling and heating functions. For example, gas in the halo within 1 Mpc of this quasar will not be able to cool and condense into the disk if its virial temperature is below about 10^5 K.

HII *Region Around an O Star*

In the right panel of Figure 5, we show the cooling and heating functions for a solar metallicity cloud with density $n_b = 1\,\mathrm{cm}^{-3}$ surrounding an O star with bolometric luminosity $L = 30{,}000 L_\odot$. For the stellar spectrum, we assume a black-body with $T = 30{,}000\,\mathrm{K}$. The distances we consider are well within the star's Strömgren radius ($\sim 30\,\mathrm{pc}$), so we may safely assume that the radial dependence of the starlight is $1/r^2$ (no depletion due to recombinations). If, instead of a single star, we consider a cluster of N O stars, our result will still hold if we simply rescale the distance axis by $N^{1/2}$.

Close enough to the star, the equilibrium temperature of the HII region can be substantially higher than the canonical 10^4 K.

Quasar Irradiating its own Halo

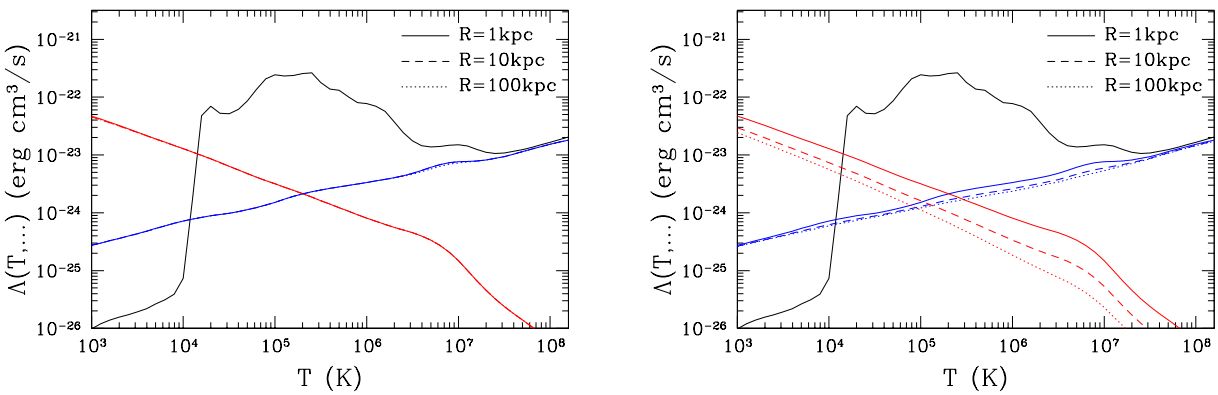

FIG. 6.— Cooling (blue lines) and heating (red lines) curves for a halo with a $z = 3$ isothermal density profile surrounding a quasar with $10^{13} L_\odot$ in ionizing radiation. In the left panel, the metallicity is fixed at $0.5 Z_\odot$, in which case the cooling and heating functions become distance-independent. In the right panel, the metallicity has a mild outward gradient, $Z \propto r^{-1/2}$. The black solid curves show the pure CIE "standard cooling function".

In Figure 6 we show cooling and heating functions in a gaseous halo at $z = 3$ (virial density $n_b = 200 \times \bar{n}_b = 3.2 \times 10^{-3}\,\mathrm{cm}^{-3}$) irradiated by a $\sim 10^9 M_\odot$ central black hole ($10^{13} L_\odot$ in ionizing radiation). The density profile of the cloud is taken as

$$n_b = 3.2 \times 10^{-3}\,\mathrm{cm}^{-3} \left(\frac{100\,\mathrm{kpc}}{r}\right)^2$$

and the metallicity is taken either to be constant $0.5 Z_\odot$ (leading to distance-independent heating and cooling functions) or to have a mild outward gradient,

$$Z = 0.5 Z_\odot \left(\frac{1\,\mathrm{kpc}}{r}\right)^{1/2}.$$

In both cases, the quasar is capable of maintaining the heating rate in excess of the cooling rate for $T \lesssim 10^5$ K. It is therefore possible to prevent cooling in the halo – and hence, accretion of fresh gas onto the galactic disk and the black hole – without any need for a mechanical or non-radiative thermal feedback mechanism.

REFERENCES

Benjamin, R. A., Benson, B. A., & Cox, D. P. 2001, ApJ, 554, L225
Benson, A. J., Lacey, C. G., Baugh, C. M., Cole, S., & Frenk, C. S. 2002, MNRAS, 333, 156
Boehringer, H. & Hensler, G. 1989, A&A, 215, 147
Cox, D. P. & Tucker, W. H. 1969, ApJ, 157, 1157
Draine, B. T. 1978, ApJS, 36, 595
Ferland, G. J., Korista, K. T., Verner, D. A., Ferguson, J. W., Kingdon, J. B., & Verner, E. M. 1998, PASP, 110, 761
Gaetz, T. J. & Salpeter, E. E. 1983, ApJS, 52, 155
Gnat, O. & Sternberg, A. 2007, ApJS, 168, 213
Haardt, F. & Madau, P. 2001, in Clusters of Galaxies and the High Redshift Universe Observed in X-rays, ed. D. M. Neumann & J. T. V. Tran
Kravtsov, A. V. 2003, ApJ, 590, L1
Landi, E. & Landini, M. 1999, A&A, 347, 401
Leitherer, C., Schaerer, D., Goldader, J. D., Delgado, R. M. G., Robert, C., Kune, D. F., de Mello, D. F., Devost, D., & Heckman, T. M. 1999, ApJS, 123, 3
Mathis, J. S., Mezger, P. G., & Panagia, N. 1983, A&A, 128, 212
Raymond, J. C., Cox, D. P., & Smith, B. W. 1976, ApJ, 204, 290
Ricotti, M., Gnedin, N. Y., & Shull, J. M. 2002, ApJ, 575, 33
Santoro, F. & Shull, J. M. 2006, ApJ, 643, 26
Shull, J. M. & van Steenberg, M. 1982, ApJS, 48, 95
Smith, B., Sigurdsson, S., & Abel, T. 2008, MNRAS, 385, 1443
Sutherland, R. S. & Dopita, M. A. 1993, ApJS, 88, 253
Vasiliev, E. O. 2011, MNRAS, 414, 3145
Wiersma, R. P. C., Schaye, J., & Smith, B. D. 2009, MNRAS, 393, 99